ARTICLE

Prediction Model of Wax Deposition Rate in Waxy Crude Oil Pipelines by Elman Neural Network Based on Improved Reptile Search Algorithm

Zhuo Chen[1,*], Ningning Wang[2], Wenbo Jin[3] and Dui Li[1]

[1]The Second Oil Production Plant, Sinopec Northwest Oilfield Company, Urumqi, 830011, China

[2]Yingmaili Oil and Gas Production Management Area, PetroChina Tarim Oilfield Company, Korla, 841001, China

[3]College of Petroleum Engineering, Xi'an Shiyou University, Xi'an, 710065, China

[*]Corresponding Author: Zhuo Chen. Email: 18691298736@163.com

ABSTRACT

A hard problem that hinders the movement of waxy crude oil is wax deposition in oil pipelines. To ensure the safe operation of crude oil pipelines, an accurate model must be developed to predict the rate of wax deposition in crude oil pipelines. Aiming at the shortcomings of the ENN prediction model, which easily falls into the local minimum value and weak generalization ability in the implementation process, an optimized ENN prediction model based on the IRSA is proposed. The validity of the new model was confirmed by the accurate prediction of two sets of experimental data on wax deposition in crude oil pipelines. The two groups of crude oil wax deposition rate case prediction results showed that the average absolute percentage errors of IRSA-ENN prediction models is 0.5476% and 0.7831%, respectively. Additionally, it shows a higher prediction accuracy compared to the ENN prediction model. In fact, the new model established by using the IRSA to optimize ENN can optimize the initial weights and thresholds in the prediction process, which can overcome the shortcomings of the ENN prediction model, such as weak generalization ability and tendency to fall into the local minimum value, so that it has the advantages of strong implementation and high prediction accuracy.

KEYWORDS

Waxy crude oil; wax deposition rate; chaotic map; improved reptile search algorithm; Elman neural network; prediction accuracy

Nomenclature

X_1	Flow velocity/(m.s^{-1})
X_2	Oil temperature/°C
X_3	Wall temperature/°C
X_4	Shear stress at pipe wall/Pa
X_5	Crude oil viscosity/(mPa·s)
X_6	Wax molecular concentration gradient at pipe wall/(10^{-3}·°C^{-1})
X_7	Temperature gradient at pipe wall/(°C·mm^{-1})
X_8	Wax deposition rate/(g·m^{-2}·h^{-1})
Y_1	Oil temperature/°C
Y_2	Wall temperature/°C

Y_3	Crude oil viscosity/(mPa·s)
Y_4	Shear stress at pipe wall/Pa
Y_5	Flow velocity/(m·s^{-1})
Y_6	Temperature gradient at pipe wall/(°C·mm^{-1})
Y_7	Wax molecular concentration gradient at pipe wall/(10^{-3}·°C^{-1})
Y_8	Wax deposition rate/(g·m^{-2}·h^{-1})
P	Predicted value/(g·m^{-2}·h^{-1})
R	Relative error/%

*Note: Variables X_1 to X_8 represent wax deposition rate data from the Kenli Oilfield, and variables Y_1 to Y_8 represent wax deposition rate data from the Huachi operation area.

ENN	Elman neural network
IRSA	Improved reptile search algorithm
RSA	Reptile search algorithm
BPNN	Back-propagation neural network
RBF	Radial basis function
MLP	Multilayer perceptron
MLP-LMA	Multilayer perceptron Levenberg-Marquardt algorithm
CFNN	Cascaded forward neural network
GRNN	Generalized regression neural network
PWLCM	Piecewise linear chaotic map
N	Number of hidden layer nodes
MSE	Mean square error
RMSE	Root mean square error
MAPE	Mean absolute percentage error
R^2	Correlation coefficient
m	Number of nodes in the input layer
n	Number of nodes in the output layer
a	Integers between 1 and 10
WOA	Whale optimization algorithm
HUANG	Huang Qiyu wax deposition prediction model

1 Introduction

Pipeline wax deposition is a common problem when crude oils are transported in pipelines. Crude oils produced in China tend to have a high viscosity, coagulate easily, and contain high levels of wax. During the transportation of waxy crude oil through pipelines, changes in pressure and temperature conditions promote the precipitation of solid heavy constituents, including waxes, colloids, and asphaltenes, resulting in the formation of wax deposits on the pipeline walls [1–3]. The oil produced from an oilfield in China is shown in Fig. 1.

Wax deposition reduces the effective flow area of the pipeline, increasing flow resistance, reducing transport capacity, and in severe cases, even causing pipeline blockage and destructive accidents [4–6]. Therefore, it is crucial to accurately understand the mechanism of wax deposition during crude oil pipeline transportation and calculate the rate of wax deposition in the pipeline. This holds significant practical importance for ensuring safe oil well production. The wax deposition phenomenon of crude oil pipelines in oilfield engineering practice is shown in Fig. 2.
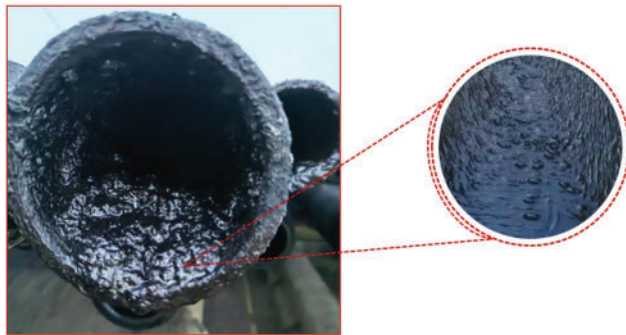
Figure 1: The oil produced from an oilfield in China

Figure 2: Wax deposition in crude oil pipeline

Researchers simulated the wax deposition phenomenon in pipelines through experiments, combined with theoretical analysis to summarize the influence mechanism of wax deposition, and established prediction models for wax deposition to predict the actual wax deposition [7–11]. Currently, prediction models for wax deposition rate generally consist of the thermodynamic prediction model, kinetic prediction model, and artificial intelligence prediction model [12–14].

1) Thermodynamic prediction model

The relevant theories affecting wax deposition have been introduced by researchers, who utilized thermodynamics, colloid chemistry, and hydrodynamics to conduct extensive experiments, theoretical analyses, and summarize a representative Thermodynamic mathematical model of wax deposition. However, the components contained in the solid phase of wax deposition are very complex, and the properties of the components are quite different, which leads to the complexity of the model formula, poor adaptability, narrow application range, limited accuracy, and inconvenient application [15].

2) Dynamic prediction model

Combined with the wax deposition mechanism of crude oil pipelines and the influence of various conditions and factors, researchers established the prediction model of wax deposition dynamics based on "The Law of Fick Diffusion" and determined the relevant parameters of the model through experiments. This kind of model is characterized by simple application and can reflect the wax

deposition in the actual pipeline to a certain extent, but the prediction accuracy still has a lot of room for improvement [16,17].

3) Artificial intelligence prediction model

The fast development of computer science provides a new way of thinking about wax deposition prediction. This method does not need to consider various mechanisms and complicated influencing factors affecting wax deposition, but only needs to establish enough experimental data samples, then combine artificial intelligence methods to learn the experimental data samples, and then a trained artificial intelligence wax deposition prediction model can be constructed. This method can be used to predict the wax deposition in other operating conditions [18,19].

Zhou et al. [20] examined the effect of different factors on the wax deposition rate of pipelines and established a prediction model for the BPNN wax deposition model by error back-propagation neural network (BPNN). Coto et al. [21] established a novel predictive model for wax deposition in pipelines and compared it with laboratory measurements, which has the advantage of high prediction accuracy. Tian et al. [22] considered the effects of seven factors on the rate of wax deposition in pipelines and established a 7-10-1 three-layer neural network structure using the BPNN model. The results show that the BPNN model itself has some inherent defects, which will greatly affect the prediction performance. Wang et al. [23] established a novel prediction model for pipeline wax deposition rate using support vector machine (SVM) model. The authors pointed out that different combinations of the penalty factor C and the kernel function parameter g have a great impact on the prediction results when the radial basis function (RBF) neural network is used as the kernel function. Xie et al. [24] established an RBF neural network wax deposition rate prediction model. The relative error of the model is only 1.5% compared with the experimental data. Lashkarbolooki et al. [25] established a novel multilayer perceptron (MLP) wax deposition prediction model, and compared with the experimental data, the newly constructed model has higher prediction accuracy. Behnam et al. [26] established four models to predict wax deposition rates in crude oil pipelines using pour point temperature and °API as the main factors affecting wax deposition: MLP, RBF, CFNN, and GRNN. The results showed that the GRNN model has a stronger predictive capability. The models and methods proposed by the above scholars have unique advantages, but due to the limitations of optimization algorithms (it is impossible to achieve the best balance between global optimum and local optimum) and neural networks, it may lead to the inability to accurately predict the wax deposition rate of waxy crude oil pipelines for multi-factor and high-dimensional problems.

As a widely used neural network, ENN has a real-time feedback function and short-term memory capability (adding a context layer to the traditional three-layer network structure) [27,28]. Compared with BPNN, ENN is better in network stability and calculation accuracy, but it also has some defects (lack of generalization ability, easy to fall into the local minimum value). How to improve it through related optimization algorithms is still an important content of current research. The Reptile Search Algorithm (RSA) is a novel meta-heuristic algorithm, which has the advantages of high solution accuracy and fast operation speed [29–31]. In the application of RSA, a difficult problem is how to get the best balance between global search and local search. In fact, this is also a shortcoming of the algorithm. Considering the advantages of RSA and the shortcomings of current research, this paper introduces the strategy of Piecewise Linear Chaotic Map (PWLCM) (enriching population exploration space), proposes an IRSA, constructs the IRSA-ENN model, and verifies the validity of the new model by predicting the wax deposition rate of two groups of waxy crude oil measured data. The research results have important guiding significance for the accurate prediction of the wax deposition rate of waxy crude oil pipeline.

2 Theoretical Basis

2.1 Bellman Neural Network Model

ENN is a type of local regression network with a local memory unit and a local feedback connection. Different from BPNN, it adds a context layer based on the traditional three-layer network structure, so it has the characteristics of memory. Its structure is schematically shown in Fig. 3.
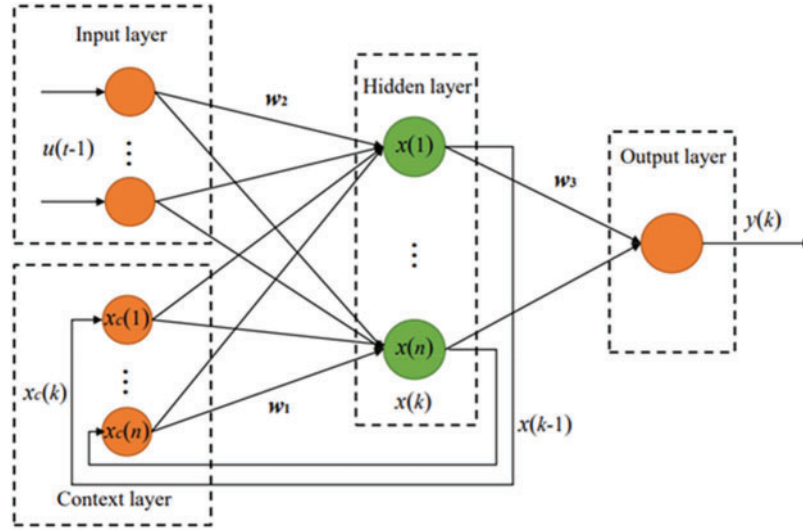

Figure 3: Elman neural network structure

The nonlinear state space expression of ENN is shown in Eq. (1).

$$\begin{cases} y(k) = P(w_3 x(k)) \\ x(k) = Q(w_1 x_c(k)) + w_2(u(k-1)) \\ x_c(k) = x(k-1) \end{cases} \tag{1}$$

where: k represents the time; $y(k)$ is the output vector of the output node unit; $x(k)$ is the output vector of the middle layer; $a_c(k)$ is the output of the context layer; u is the input layer unit vector; w_1 represents the weight matrix of the context and hidden layers; w_2 represents the weight matrix of the input and hidden layers; w_3 represents the weight matrix of the output and hidden layers; $P()$ is the transfer function of the output neuron; $Q()$ is the transfer function of middle layer neurons, the sigma function is used in this paper [32], as shown in Eq. (2).

$$Q(x) = \frac{1}{1 + e^{-x}} \tag{2}$$

When ENN updates the weights and thresholds, it actually uses error back-propagation and the error square sum function to measure them, as shown in Eq. (3).

$$E(k) = \frac{1}{2}\left[(y_d(k) - y(k))^T (y_d(k) - y(k))\right] \tag{3}$$

where: $E(k)$ represents the sum of squares of errors; $y_d(k)$ is the actual output matrix of the neural network at the k-th time; $y(k)$ is the network prediction output matrix at the k-th time; T is the transpose matrix.

2.2 Improved Reptile Search Algorithm

RSA, as a novel intelligent optimization algorithm, is superior to the traditional optimization algorithm in terms of high precision and fast computing speed. However, when applied to high-dimensional feature selection problems, RSA will be affected by population diversity. In order to overcome this shortcoming, PWLCM is utilized to enhance the population's exploration ability in the search range, and an IRSA is proposed.

Specifically, IRSA is a coupling algorithm that takes advantage of PWLCM to enhance population diversity. In IRSA, PWLCM is used to enrich the ability of the RSA population to explore the spatial domain, thereby improving its ability to solve high-dimensional and complex nonlinear optimization problems.

2.2.1 Reptile Search Algorithm

RSA is a novel meta-heuristic algorithm proposed by Abualigah et al. It is a population-based and gradient-free algorithm established by studying the social behavior, prey encircling mechanism, and hunting mechanism of crocodiles in nature. The algorithm is mainly divided into three main stages: initialization, prey encircling, and hunting. In the calculation process, the prey encircling stage and the hunting stage can be alternated continuously, thus narrowing the search range and catching prey.

The detailed principle of RSA has been described in the literature, which will not be repeated in the article [29–31]. The RSA optimization process is divided into two phases: the exploration phase and the exploitation phase, which are described as follows:

1) Exploration phase [Encircling]

When reptiles encircle their prey, they have two walking modes (high walking and low creeping walking), as shown in Fig. 4, and the mathematical expression is shown in Eq. (4).

$$X_{(i,j)}(t+1) = \begin{cases} Best_j(t) - C_{(i,j)}(t) \times \beta - R_{(i,j)}(t) \times rand, t \leq T/4 & (a) \\ Best_j(t) \times x_{(r1,j)} \times ES(t) \times rand, T/4 < t \leq T/2 & (b) \end{cases} \tag{4}$$

where: $Best(t)$ is the optimal solution obtained at the j position in this stage; $C_{(i,j)}$ is the hunting operator at the j position on the i result; β is the correction parameter, which controls the accuracy of the solution under the constraint condition of high walk in this stage; $R_{(i,j)}$ is a *Reduce* function, which is mainly used to narrow the search range; *rand* is a random number from 0 to 1; $x_{(r1,j)}$ is the random position of the i-Th solution; t is the current number of iteration steps; T is the maximum number of iteration steps; $ES(t)$ is the evolutionary ratio, which is the probability ratio that decreases randomly between $[-2, 2]$ in the iterative process.

2) Exploitation phase [Hunting]

In the hunting phase, reptiles have two social behaviors (coordination and cooperation), as shown in Fig. 5, and the mathematical expression is shown in Eq. (5).

$$X_{(i,j)}(t+1) = \begin{cases} Best_j(t) \times P_{(i,j)}(t) \times rand, T/2 < t \leq 3T/4 & (a) \\ Best_j(t) - C_{(i,j)}(t) \times \delta - R_{(i,j)}(t) \times rand, 3T/4 < t \leq T & (b) \end{cases} \tag{5}$$

where: $Best(t)$ is the optimal solution obtained at the j position in this stage; $C_{(i,j)}$ is the hunting operator at the j position on the i result; $P_{(i,j)}$ is the percentage of the difference between the best solution at the j-th position and the current solution; *rand* is a random number from 0 to 1; δ is a small value.
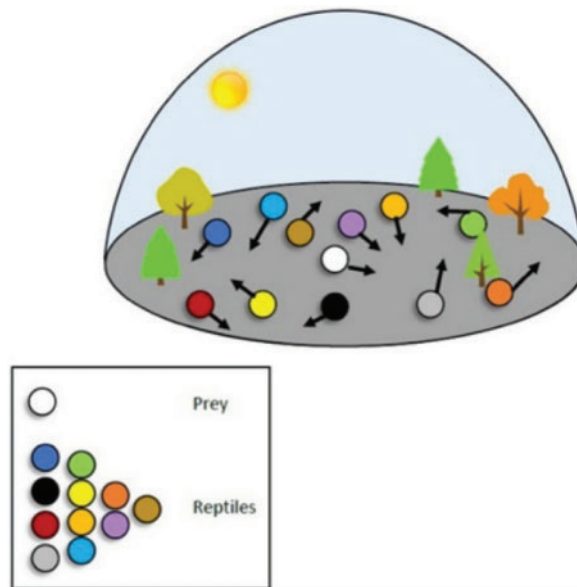
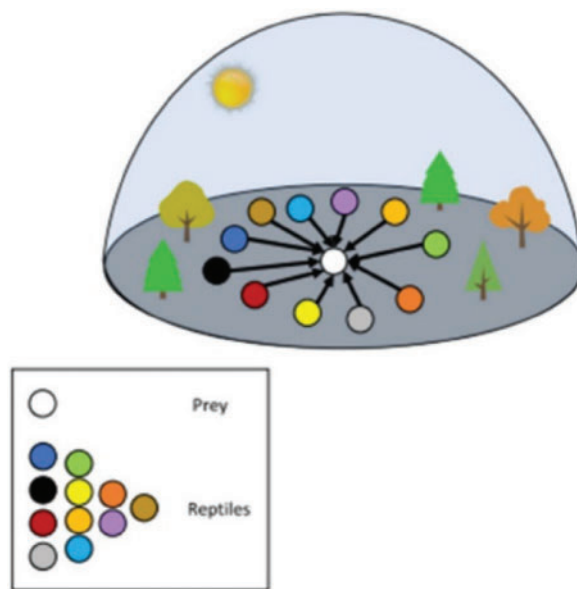**Figure 4:** Reptiles encircling the prey [29]

Figure 5: Reptiles attacking the prey [29]

2.2.2 Piecewise Linear Chaotic Map

Chaotic mapping is an effective method to deal with the problem of population diversity and low convergence speed in optimization algorithms. In this paper, PWLCM is used to initialize the population position, and then expand the search space, so as to improve the performance of RSA. As a typical representative of chaotic mapping, PWLCM has a simple mathematical form, ergodicity, and randomness. The mathematical expression is shown in Eq. (6).

$$x(t+1) = \begin{cases} \dfrac{x(t)}{p}, 0 \le x(t) < p \\ \dfrac{x(t)-p}{0.5-p}, p \le x(t) < 0.5 \\ \dfrac{1-p-x(t)}{0.5-p}, 0.5 \le x(t) < 1-p \\ \dfrac{1-x(t)}{p}, 1-p \le x(t) < 1 \end{cases} \qquad (6)$$

where: p is a control parameter, which is used to determine the section range of the four-section formula so that there is no overlap between them, and the range is $(0, 0.5)$. $x(t)$ is the generated random iterative value in the range of $[0,1]$.

2.2.3 Comparison before and after Algorithm Improvement

In this paper, the RSA original method and PWLCM are used to initialize the population, and the results of random initialization of the population sequence are compared to verify whether PWLCM can explore the population space more thoroughly [30,31]. To conveniently compare the results, the number of particles is set to 150, the maximum number of iterations is 50, and the value of p in PWLCM is 0.4.

Comparing Figs. 6 with 7, it can be seen that the random initialization strategy of the PWLCM effectively enhances the ergodicity of the population and avoids the large blank of the population in the search range.
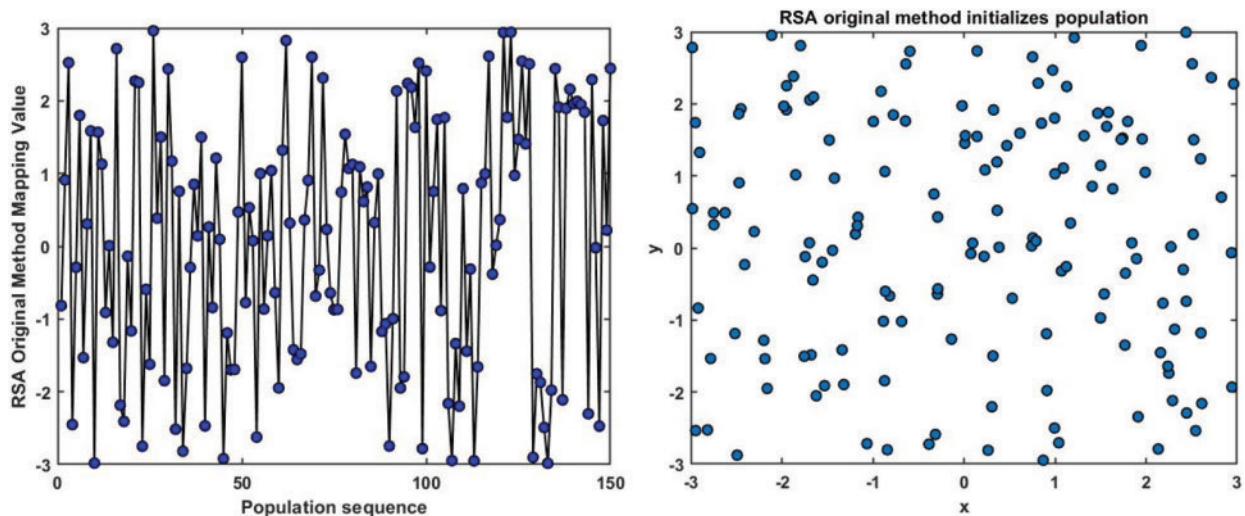

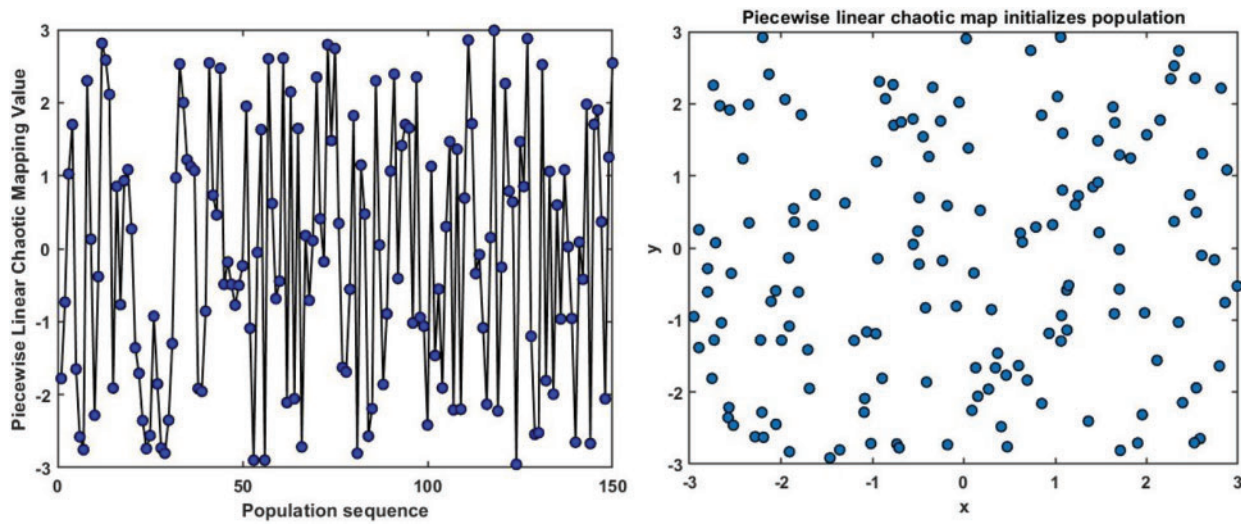**Figure 6:** The RSA original method randomly initializes the population

Figure 7: PWLCM randomly initializes the population

3 Wax Deposition Rate Prediction Model for Crude Oil Pipelines Based on IRSA-ENN Algorithm

3.1 Construction of IRSA-ENN Model

The construction process of the wax deposition rate prediction model for waxy crude oil pipelines based on the IRSA-ENN prediction model is shown in Fig. 8.
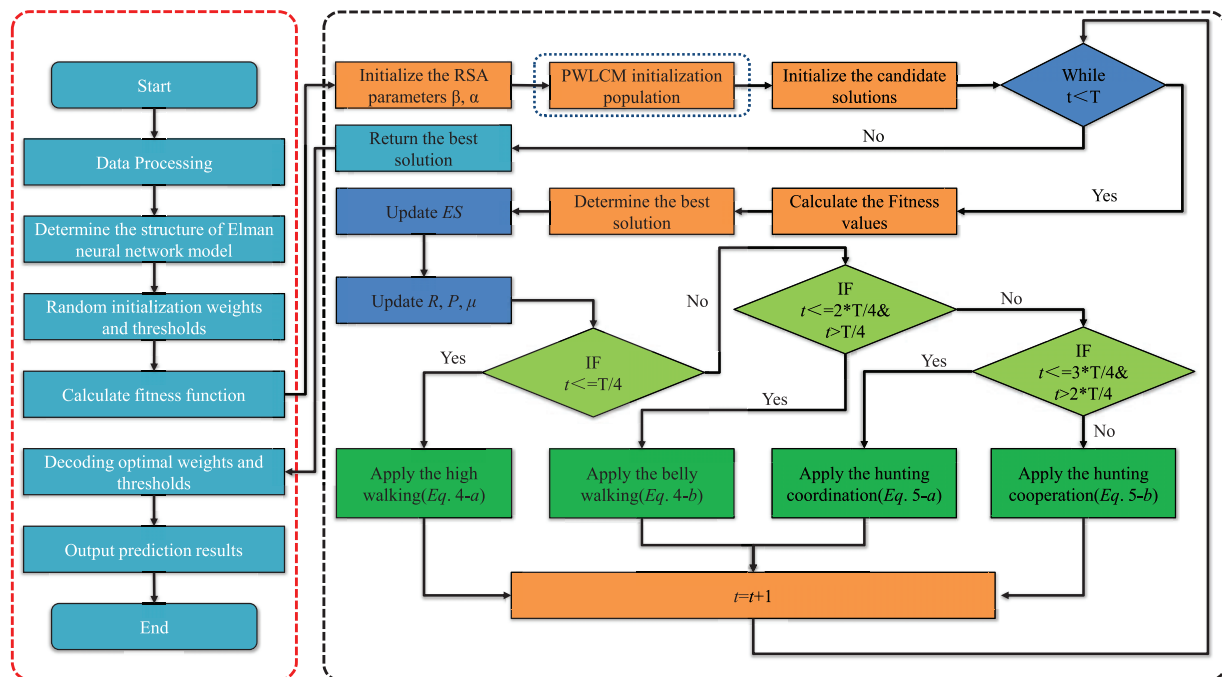

Figure 8: Wax deposition rate model for pipelines with waxy crude oil based on IRSA-ENN algorithm

The IRSA is applied to optimize the ENN model, thus constructing the IRSA-ENN prediction model. The model constructed by this method can overcome the problems of low prediction accuracy and insufficient generalization ability of the ENN model. The steps of establishing the model are as follows.

Step 1: The experimental data on wax deposition rates in crude oil pipelines have been normalized to initialize the ENN model and determine the number of input hidden and output layers. The IRSA is introduced to set the initial parameters (including population number, iteration times, problem dimension, etc.).

Step 2: PWLCM (Eq. (6)) is introduced to initialize the reptile population sequence and randomly distribute the reptile exploration space. The fitness function (MSE of training samples) is calculated (Eq. (7)) to measure the optimal solution in the overall optimization process.

$$fitness = \frac{1}{n} \sum_{i=1}^{n} \left(d_{fi} - d_{vi} \right)^2 \tag{7}$$

where: d_{fi} is the output value of the i-th sample model; d_{vi} is the actual value of the i-th sample.

Step 3: According to the updated position of the reptile, the fitness function of the reptile at this position is obtained, and the position of the reptile is updated by Eqs. (4) and (5), that is to adjust the threshold and weight of ENN. Then, compared with the current position fitness value and the current optimal value. If the current position fitness value is better, it is updated, otherwise it is not updated.

Step 4: Generation of the optimal solution. When the iteration of the algorithm stops, the final optimal solution is the optimal solution of the whole training.

Step 5: The optimal solution (optimal weights and thresholds of the ENN) is assigned to the ENN model, and the improved ENN model is trained after matrix reconstruction and predicted from the experimental data of pipeline wax deposition rate.

3.2 Model Evaluation

Three evaluation parameters, RMSE, MAPE, and R^2, are introduced to evaluate the prediction accuracy of the model [33]. The calculation Eqs. (8)–(10) of the three are as follows:

$$RMSE = \sqrt{\frac{1}{M} \sum_{i=1}^{M} \left(y_i - f\left(x_i \right) \right)^2} \tag{8}$$

$$MAPE = \frac{1}{M} \sum_{i=1}^{M} \left| \frac{y_i - f\left(x_i \right)}{y_i} \right| \times 100\% \tag{9}$$

$$R^2 = \frac{\sum_{i=1}^{M} \left(y_i - \bar{y} \right) \cdot \left(f\left(x_i \right) - \bar{f} \right)}{\sqrt{\sum_{i=1}^{M} \left(y_i - \bar{y} \right)^2 \sum_{i=1}^{M} \left(f\left(x_i \right) - \bar{f} \right)^2}} \tag{10}$$

where: M represents the number of sample sets; y_i is the actual value; $f(x_i)$ is the predicted value; $\bar{y}$ is the average value of the actual value; and $\bar{f}$ is the average of predicted values.

4 Proposed ENN Modelling and Analysis

4.1 Data Acquisition and Preprocessing

Two groups of measured wax deposition rate data of crude oil pipelines with different physical properties given in the article [34,35] are taken as cases (corresponding to Case I and Case II respectively) to verify the generalization performance of the improved new model (learning ability for different groups of measured data), and to compare and analyze the prediction accuracy of the IRSA-ENN model and other models. The measured data of wax deposition rate in crude oil pipelines are 35 groups and 38 groups, respectively, among which 5 groups of data are randomly selected as prediction samples (the rest are used as their own training samples) to compare and analyze the prediction accuracy of each model. The measured data of wax deposition rate in two groups of different waxy crude oil pipelines are shown in Appendix A.

When learning training samples, because of the different dimensions among variables, we need to use the map min-max function to normalize the data, that is, map the data of each variable to the range of [0,1], The mathematical expression is shown in Eq. (11).

$$y_i = \frac{x_i - \min(x_i)}{\max(x_i) - \min(x_i)} \tag{11}$$

where: y_i represents the processed sample data; x_i represents preprocessing data.

4.2 Result Analysis and Model Evaluation

MATLAB software is used to realize the simulation process, and the parameters of the computer are shown in Table 1. The ENN model determines the optimal number of hidden layer nodes by minimizing the MSE of the training samples as a measure of the machine learning on the training samples of Case 1 and Case 2. The learning parameters of the ENN model are shown in Table 2. When the ENN model determines the optimized number of hidden layer nodes H for the wax deposition rate data of the pipelines in Case 1 and Case 2, the formula is Eq. (12).

$$H = \sqrt{m + n} + a \tag{12}$$

where: The value of H varies with the value of a.

Table 1: Computer software and hardware parameters

Name	Detailed parameters
Central processing unit (CPU)	AMD Ryzen7 5800H @ 3. 20 GHz
ROM	32.0 GB
Operating system (OS)	Windows 11
Language	MATLAB R2020a

Table 2: ENN model learning parameters setting

Parameters	Detailed settings
Number of training sessions	1000
Learning rate	0.01

(Continued)

Table 2 (continued)

Parameters	Detailed settings
Minimum error of training target	1×10^{-6}
Momentum factor	0.01
Minimum performance gradient	1×10^{-6}

The MSE results of training samples solved by different hidden layer nodes in Case I and Case II are shown in Tables 3 and 4.

Table 3: Calculation of the MSE of training samples with different numbers of hidden layer nodes (Case I)

N	3	4	5	6	7	8	9	10	11	12
MSE	0.1233	0.0399	0.3131	0.0330	0.0237	0.5582	0.4852	0.0157	0.0079	0.0348

Table 4: Calculation of the MSE of training samples with different numbers of hidden layer nodes (Case II)

N	3	4	5	6	7	8	9	10	11	12
MSE	0.2431	0.1701	0.3874	0.1382	0.0137	0.2362	0.1563	0.2708	0.0181	0.3871

As shown in Table 3, when the number of hidden layer nodes is 11, the MSE of the training samples is minimized (Case 1), so Case 1 is determined to construct a 7-11-1 three-layer ENN model. Similarly, as shown in Table 4, when the number of hidden layer nodes is 7, the MSE of the training samples is minimized (Case 2), so Case 2 is determined to construct the 7-7-1 three-layer ENN model.

To validate the prediction accuracy of the IRSA-ENN, Huang Qiyu wax deposition prediction (HUANG), ENN, Whale optimization algorithm-ENN (WOA-ENN), and RSA-ENN models are established and compared [36,37]. For easy comparison and analysis of the forecast results, fixed random seeds are used to ensure the consistency of each running result of each model, the iterative optimization times of each model are set to 150 times and the population size is 50. The initialization constants of the WOA-ENN model are $a = [0,2]$, $b = 1$, $l = [-1,1]$. The initialization constants of RSA-ENN and IRSA-ENN are $\alpha = 0.1$ and $\beta = 0.005$. The results of the predictions of various models for the two wax deposition rate Cases are shown in Tables 5–7, Figs. 9 and 10, along with the relative error results.

Table 5: Prediction results and relative errors of different models (Case I)

No.	Actual value	HUANG		ENN		WOA-ENN		RSA-ENN		IRSA-ENN	
		P	R	P	R	P	R	P	R	P	R
1	17.033	18.557	8.9522	18.4059	8.0600	16.9269	0.6232	16.9465	0.5078	17.0145	0.1087
2	21.261	22.452	5.6059	22.7987	7.2324	21.2828	0.1027	21.1630	0.4611	21.3387	0.3653
3	28.390	27.455	2.9935	31.2323	10.0116	28.7643	1.3184	28.2890	0.3559	28.3989	0.0314
4	22.837	23.578	3.2471	25.1524	10.1388	23.1690	1.4539	22.9192	0.3598	22.8118	0.1103
5	13.575	15.331	12.935	16.1136	18.7004	13.5874	0.0916	13.5865	0.0844	13.4660	0.8032

Table 6: Prediction results and relative errors of different models (Case II)

No.	Actual value	HUANG		ENN		WOA-ENN		RSA-ENN		IRSA-ENN	
		P	R	P	R	P	R	P	R	P	R
1	12.11	16.213	33.884	12.0819	0.2319	12.2489	1.1469	12.140	0.2558	12.0338	0.6290
2	9.60	9.392	2.1661	8.8676	7.6295	9.5700	0.3127	9.5956	0.0454	9.6023	0.0241
3	8.66	6.371	26.426	8.6799	0.2296	8.5769	0.9595	8.7492	1.0301	8.6527	0.0848
4	18.09	24.025	32.813	18.9128	4.5482	17.9921	0.5411	17.7921	1.6469	18.2355	0.8045
5	16.43	13.512	17.759	21.2316	29.2244	16.6630	1.4179	16.5435	0.6911	16.4846	0.3325

Table 7: Comparison of prediction accuracy of different models

Case I				Case II			
Model	MAPE/%	RMSE	R^2	Model	MAPE/%	RMSE	R^2
HUANG	6.7469	/	0.99127	HUANG	22.609	/	0.63418
ENN	10.8286	2.1970	0.98660	ENN	8.3727	2.2032	0.88435
WOA-ENN	0.7180	0.2290	0.99941	WOA-ENN	0.8756	0.1349	0.99849
RSA-ENN	0.3538	0.0826	0.99973	RSA-ENN	0.7338	0.1487	0.99847
IRSA-ENN	0.2837	0.0616	0.99988	IRSA-ENN	0.3749	0.0774	0.99977

It can be seen from Tables 5–7, Figs. 9 and 10 that the IRSA-ENN model has higher prediction accuracy than the HUANG, RSA-ENN, WOA-ENN, and ENN models, and its correlation coefficient R^2 is closer to 1, and its MAPE is only 0.2837% and 0.3749%, respectively, which is smaller than other models. In addition, the prediction accuracy of WOA-ENN and RSA-ENN models for two groups of waxy crude oil wax deposition rate is obviously higher than that of the ENN model, which further proves the effectiveness of using an optimization algorithm to improve the ENN model. Generally speaking, the IRSA-ENN model has ideal results for predicting wax deposition rate data of different groups of crude oil. The model is suitable for describing wax deposition in waxy crude oil pipelines

in the petroleum industry and has a certain guiding significance for guiding the pigging of crude oil pipelines.
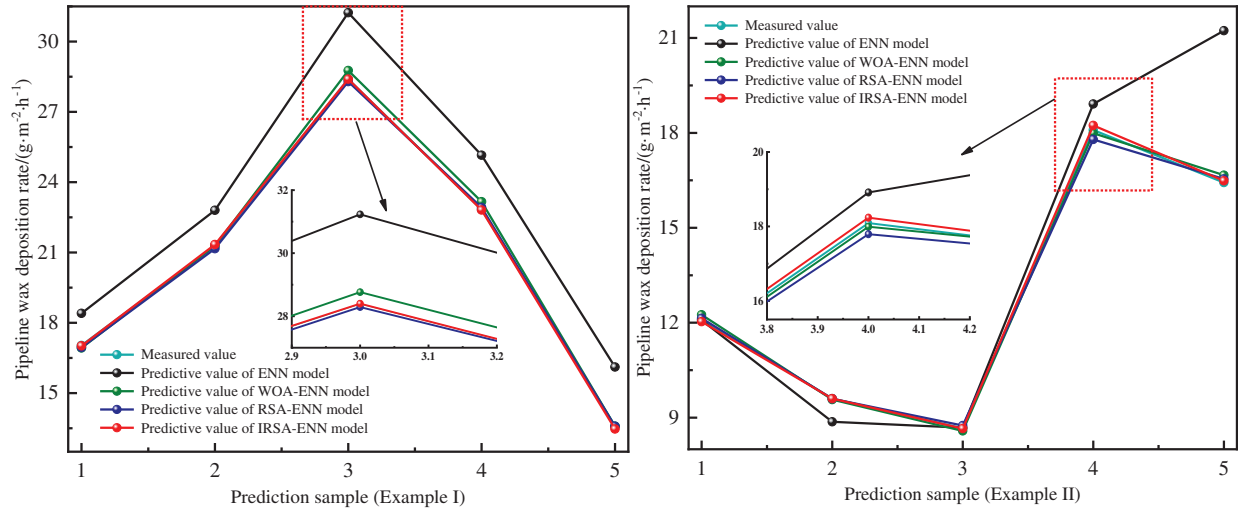

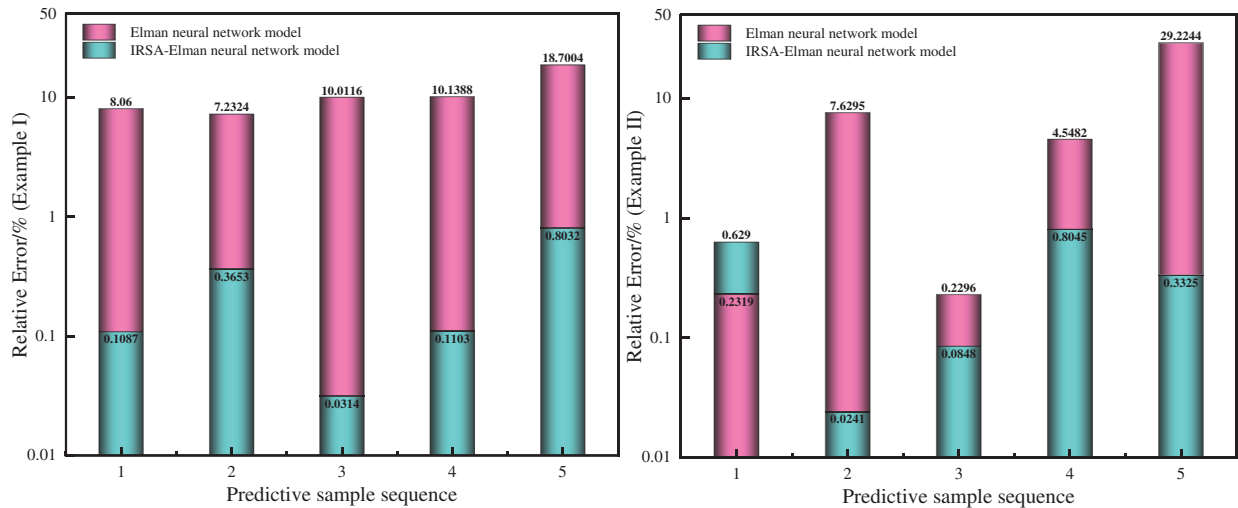**Figure 9:** Comparison of prediction results of different models

Figure 10: Comparison of prediction errors between IRSA-ENN and ENN models

According to the prediction results of wax deposition in two groups of crude oil pipelines by the ENN model, the prediction accuracy is poor. This is due to the fact that the Elman trains function of the ENN model uses the BP training function to modify the weights, which leads to the defect that the gradient descent method easily falls into local minima when solving the partial derivative of $E(k)$ to the weights. When the ENN is used to create the prediction model, the initial weights and thresholds are usually initialized by pseudo-random numbers, which leads to the poor stability of the trained prediction model, and then leads to the lack of generalization ability (the adaptability of training and learning to new samples).

The improved ENN model can be globally optimized for the randomly initialized weights and thresholds, which is beneficial to: (1) overcoming as much as possible the defects of slow convergence speed and easily falls into local minima when the ENN model is adjusted by the gradient descent method in the training process due to improper initial weights and thresholds; (2) it avoids the defect that when using the random method to assign weights and thresholds, it is easy to lead to a well-trained model, and it is difficult to obtain accurate prediction results when predicting other samples, and improving the generalization ability of ENN model.

In addition, according to the results of IRSA-ENN and RSA-ENN for waxy crude oil pipeline wax deposition prediction, the MAPE and RMSE of RSA-ENN for Case I are 0.3538% and 0.0826%, respectively, and the MAPE and RMSE for Case II are 0.7338% and 0.1487%, respectively. The MAPE and RMSE of the IRSA-ENN model for Case I are 0.2837% and 0.0616%, respectively, and the MAPE and RMSE for Case II are 0.3749% and 0.0774%, respectively. Compared with the RSA-ENN model, the IRSA-ENN model has higher prediction accuracy and has more obvious advantages in the wax deposition rate of crude oil pipelines. This also proves the effectiveness of using PWLCM to improve the RSA. The reason is that the PWLCM can initialize the population sequence more randomly, and then expand the search space of the population, which overcomes the defect of insufficient global search ability of RSA in the initial stage of iterative optimization to a certain extent.

5 Conclusion

Aiming at the problem of wax deposition rate prediction of crude oil pipelines, a new method based on the IRSA-ENN model for wax deposition rate prediction is proposed in this paper. The new model is trained and verified by using two sets of measured data of the wax deposition rate of crude oil pipelines with different physical properties, and the following conclusions are obtained.

1) Aiming at the deficiency of the ENN model (generalization ability is not strong, easy to fall into local minimum value), an IRSA-ENN model is proposed, and the wax deposition rate of the crude oil pipeline is predicted by two Cases. The results show that the MAPE of the IRSA-ENN prediction model is only 0.2837% and 0.3749%, respectively, which has good prediction accuracy.

2) Using PWLCM, the RSA is improved. By comparing RSA-ENN and IRSA-ENN models for two groups of wax deposition rate prediction data of crude oil pipelines, it can be seen that the IRSA has better optimization performance.

3) Compared with the ENN model, WOA-ENN model, and RSA-ENN model, the prediction accuracy of the IRSA-ENN model has obvious advantages. It effectively solves the shortcomings of the ENN model, such as insufficient generalization ability, and easily falls into minimum value. This method provides a new way for accurate prediction of wax deposition rate, can effectively meet the demand of wax deposition rate prediction in crude oil pipelines under actual working conditions, and provides a new decision-making basis method for pigging cycle formulation and safety management of waxy crude oil pipeline.

Author Contributions: The authors confirm contribution to the paper as follows: study conception and design: Zhuo Chen, Wenbo Jin; data collection: Zhuo Chen, Dui Li; analysis and interpretation

of results: Zhuo Chen, Wenbo Jin, Ningning Wang, Dui Li; draft manuscript preparation: Zhuo Chen. All authors reviewed the results and approved the final version of the manuscript.

Availability of Data and Materials: Data supporting this study are included within the article.

Conflicts of Interest: The authors declare that they have no conflicts of interest to report regarding the present study.

References

1. Quan, Q., Gong, J., Wang, W., Gao, G. (2015). Study on the aging and critical carbon number of wax deposition with temperature for crude oils. *Journal of Petroleum Science and Engineering, 130,* 1–5. https://doi.org/10.1016/j.petrol.2015.03.026

2. Ballo, M. L., Liu, G. (2022). Review of wax sedimentations prediction models for crude-oil transportation pipelines. *Petroleum Research, 7(2),* 220–235. https://doi.org/10.1016/j.ptlrs.2021.09.005

3. Asger, B. H., Elfinn, L., Walther, B. P., Anne, B. N., Hans, P. R. (1991). Wax precipitation from North Sea crude oils. 3. Precipitation and dissolution of wax studied by differential scanning calorimetry. *American Chemical Society, 5(6),* 914–932. https://doi.org/10.1021/ef00030a021

4. Burger, E., Perkins, T., Striegler, J. (1981). Studies of wax deposition in the trans Alaska pipeline. *Journal of Petroleum Technology, 33(6),* 1075–1086. https://doi.org/10.2118/8788-PA

5. Brown, T. S., Niesen, V. G., Erickson, D. D. (1993). Measurement and prediction of the kinetics of paraffin deposition. *SPE Annual Technical Conference and Exhibition*, SPE-26548. Huston, USA. https://doi.org/10.2118/26548-MS

6. Piroozian, A., Hemmati, M., Safari, M., Rahimi, A., Rahmani, O. et al. (2021). A mechanistic understanding of the water-in-heavy oil emulsion viscosity variation: Effect of asphaltene and wax migration. *Colloids and Surfaces A: Physicochemical and Engineering Aspects, 608,* 125604. https://doi.org/10.1016/J.COLSURFA.2020.125604

7. Ashoori, S., Sharifi, M., Masoumi, M., Salehi, M. M. (2017). The relationship between SARA fractions and crude oil stability. *Egyptian Journal of Petroleum, 26,* 209–213. https://doi.org/10.1016/j.ejpe.2016.04.002

8. Arjun, J., Lu, Y. D., Sriram, R., Sarica, C., Daraboina, N. (2019). Influence of operating temperatures on long-duration wax deposition in flow lines. *Journal of Petroleum Science and Engineering, 184,* 106373. https://doi.org/10.1016/j.petrol.2019.106373

9. Shaik, N. B., Pedapati, S. R., Taqvi, S. A., Othman, A. R., Dzubir, F. A. (2020). A feed-forward back propagation neural network approach to predict the life condition of crude oil pipeline. *Processes, 8(6),* 661. https://doi.org/10.3390/pr8060661

10. Shaik, N. B., Pedapati, S. R., Othman, A. R., Bingi, K., Dzubir, F. A. (2021). An intelligent model to predict the life condition of crude oil pipelines using artificial neural networks. *Neural Computing and Applications, 33,* 14771–14792. https://doi.org/10.1007/s00521-021-06116-1

11. Wang, Z. H., Liu, Y., Li, J. X., Zhuge, X. L., Zhang, L. (2016). Study on two-phase oil-water gelling deposition behavior in low-temperature transportation. *Energy & Fuels, 30,* 4570–4582. https://doi.org/10.1021/acs.energyfuels.6b00294

12. Zhao, J., Xi, X., Dong, H., Wang, Z., Zhuo, Z. (2022). Rheo-microscopy in situ synchronous measurement of shearing thinning behaviors of waxy crude oil. *Fuel, 323,* 124427. https://doi.org/10.2139/ssrn.3998963

13. Chen, Z., Tian, Y. Y., Zhuang, Q. (2023). Effect of gas flow rate on separation efficiency at different scaling scales of cyclone separators. *Frontiers in Heat and Mass Transfer, 20,* 1–11. https://doi.org/10.5098/hmt.20.26

14. Ochieng, F. O., Kinyanjui, M. N., Abonyo, J. O., Kiogora, P. R. (2022). Mathematical modeling of wax deposition in field-scale crude oil pipeline systems. *Journal of Mathematical Analysis and Applications, 2845221,* 1–13. https://doi.org/10.1155/2022/2845221

15. Zheng, S., Saidoun, M., Palermo, T., Mateen, K., Fogler, H. S. (2017). Wax deposition modeling with considerations of non-Newtonian characteristics: Application on field-scale pipeline. *Energy & Fuels, 31,* 5011–5023. https://doi.org/10.1021/ACS.ENERGYFUELS.7B00504

16. Zhou, Y., Gong, J., Wang, P. (2016). Modeling of wax deposition for water-in-oil dispersed flow. *Asia-Pacific Journal of Chemical Engineering, 11,* 108–117. https://doi.org/10.1002/APJ.1948

17. Couto, G., Chen, H., Dellecase, E., Sarica, C., Volk, M. (2008). An investigation of two-phase oil/water paraffin deposition. *SPE Production & Operations, 23(1),* 49–55. https://doi.org/10.4043/17963-MS

18. Faysal, A., Adhreena, M., Vorathin, E., Hafizi, Z. M., Ngui, W. K. (2021). Leak diagnosis of pipeline based on empirical mode decomposition and support vector machine. *IOP Conference Series: Materials Science and Engineering, 1078,* 012023. https://doi.org/10.1088/1757-899X/1078/1/012023

19. Shaik, N. B., Pedapati, S. R., Abd Dzubir, F. A. (2020). Remaining useful life prediction of crude oil pipeline by means of deterioration curves. *Process Safety Progress, 39.* https://doi.org/10.1002/prs.12112

20. Zhou, S. D., Wu, M., Wang, J. (2004). Wax deposition rate model for crude oil pipeline based on neural network. *Journal of Xi'an Shiyou University (Natural Science Edition), 19(1),* 38–40. https://doi.org/10.3969/j.issn.1673-064X.2004.01.009

21. Coto, B., Martos, C., Espada, J. J., Robustillo, M. D., Merino-García, D. et al. (2011). A new DSC-based method to determine the wax porosity of mixtures precipitated from crude oils. *Energy Fuels, 25,* 1707–1713. https://doi.org/10.1021/ef200206h

22. Tian, Z., Jin, W. B., Zhou, L., An, Y. P., Wu, H. F. (2014). Prediction of wax deposition rate in pipeline by BP neural network. *Journal of Xi'an Shiyou University (Natural Science Edition), 29(1),* 66–70. https://doi.org/10.3969/j.issn.1673-064X.2014.01.013

23. Wang, L., Tian, Z., Pu, H. T., Jin, W. B., Dong, L. (2015). Study of wax deposition rate prediction model based on support vector machines. *Applied Chemical Industry,* 73–77.

24. Xie, Y., Xing, Y. (2017). A prediction method for the wax deposition rate based on a radial basis function neural network. *Petroleum, 3(2),* 237–241. https://doi.org/10.1016/j.petlm.2016.08.003

25. Lashkarbolooki, M., Seyfaee, A., Esmaeilzadeh, F., Mowla, D. (2010). Experimental investigation of wax deposition in Kermanshah crude oil through a monitored flow loop apparatus. *Energy & Fuels, 24,* 1234–1241. https://doi.org/10.1021/EF9010687

26. Behnam, A. R., Reza, Z., Abdolhossein, H. S. (2023). Modeling wax deposition of crude oils using cascade forward and generalized regression neural networks: Application to crude oil production. *Geoenergy Science and Engineering, 224,* 211613. https://doi.org/10.1016/j.geoen.2023.211613

27. Elman, J. L. (1990). Finding structure in time. *Cognitive Science, 14,* 179–211. https://doi.org/10.1207/s15516709cog1402-1

28. Li, X. Y., Zhang, L., Wang, Z. P., Dong, P. (2019). Remaining useful life prediction for lithium-ion batteries based on a hybrid model combining the long short-term memory and Elman neural networks. *Journal of Energy Storage, 21,* 510–518. https://doi.org/10.1016/j.est.2018.12.011

29. Abualigah, L., Abd, E. M., Sumari, P., Geem, Z. W., Gandomi, A. H. (2021). Reptile search algorithm (RSA): A nature-inspired meta-heuristic optimizer. *Expert Systems with Applications, 191,* 116158. https://doi.org/10.1016/j.eswa.2021.116158

30. Almotairi, K. H., Abualigah, L. (2022). Hybrid reptile search algorithm and remora optimization algorithm for optimization tasks and data clustering. *Symmetry, 14,* 458. https://doi.org/10.3390/sym14030458

31. Elgamal, Z. M., Sabri, A. Q., Tubishat, M., Tbaishat, D., Makhadmeh, S. N. et al. (2022). Improved reptile search optimization algorithm using chaotic map and simulated annealing for feature selection in medical field. *IEEE Access, 10,* 51428–51446. https://doi.org/10.1109/ACCESS.2022.3174854

32. Shaik, N. B., Benjapolakul, W., Pedapati, S. R., Bingi, K., Thien Le, N. et al. (2022). Recurrent neural network-based model for estimating the life condition of a dry gas pipeline. *Process Safety and Environmental Protection, 164,* 639–650. https://doi.org/10.1016/j.psep.2022.06.047

33. Shaik, N. B., Inayat, M., Benjapolakul, W., Bakthavatchalam, B., Barewar, S. D. et al. (2022). Artificial neural network modeling for thermophysical behavior of mxene ionanofluids for hybrid solar photovoltaic and thermal systems applications. *SSRN Electronic Journal, 4034718*. https://doi.org/10.2139/ssrn.4034718

34. Yang, H. M. (2015). *Study on wax deposition law and paraffin inhibitor in Kenli crude oil pipeline*. Sichuan: Southwest Petroleum University (In Chinese).

35. Wang, X. L. (2010). *Prediction and analysis of wax deposition in pipeline crude oil in Huachi operation area*. Shaanxi: Xi'an Shiyou University (In Chinese). https://doi.org/10.7666/d.y1854507

36. Seyedali, M., Lewis, A. (2016). The whale optimization algorithm. *Advances in Engineering Software, 95,* 51–67. https://doi.org/10.1016/j.advengsoft.2016.01.008

37. Fadi, A., Mohammed, Z. (2020). Wax deposition and prediction in petroleum pipelines. *Journal of Petroleum Science and Engineering, 184,* 106385. https://doi.org/10.1016/j.petrol.2019.106385

Appendix A

Table 8: Training sample of experimental data of wax deposition rate of waxy crude oil in Kenli Oilfield (Case I) [34]

Number	X_1	X_2	X_3	X_4	X_5	X_6	X_7	X_8
1	0.9	48	45	15.681	26.135	0.29	4.615	9.127
2	0.9	46	43	17.352	28.919	0.37	4.619	10.353
3	0.9	39	36	30.77	51.283	1.41	4.626	24.826
4	0.9	38	35	35.264	58.773	1.78	4.626	29.116
5	0.9	35	32	67.271	136.3	3.11	4.456	20.430
6	0.9	33	30	84.27	355.428	4.01	4.623	8.585
7	0.9	32	29	85.94	385.235	4.44	4.625	5.819
8	0.9	50	45	14.383	23.972	0.29	7.614	13.505
9	0.9	49	45	14.994	24.99	0.29	6.122	11.356
10	0.9	48	38	15.681	26.135	0.84	14.814	45.629
11	0.9	45	38	18.38	30.634	0.84	10.537	33.467
12	0.9	40	38	27.406	45.677	0.84	3.103	12.578
13	0.9	48	43	15.681	26.135	0.37	7.616	15.341
14	0.9	47	42	16.461	27.434	0.41	7.616	16.006
15	0.9	44	39	19.581	32.635	0.63	7.616	20.344
16	0.9	42	37	22.707	37.845	1.25	7.614	35.270
17	0.9	40	35	27.406	45.677	1.78	7.611	43.561
18	0.9	38	33	35.264	58.773	2.65	7.607	55.782
19	0.18	48	38	3.136	26.135	0.84	8.661	58.230
20	0.18	45	38	3.676	30.634	0.84	6.168	43.643
21	0.18	40	38	5.481	45.677	0.84	1.819	17.083
22	0.18	38	35	7.053	58.773	1.78	2.713	39.127
23	0.18	48	38	7.666	26.135	0.84	11.781	51.060
24	0.44	45	38	8.986	30.634	0.84	8.391	37.855
25	0.44	42	38	11.101	37.845	0.84	4.885	24.331
26	0.44	40	38	13.399	45.677	0.84	2.475	14.515

(Continued)

Table 8 (continued)

Number	X_1	X_2	X_3	X_4	X_5	X_6	X_7	X_8
27	0.44	38	35	17.24	58.773	1.78	3.689	33.421
28	0.62	48	38	10.803	26.135	0.84	13.177	48.423
29	0.62	45	38	12.662	30.634	0.84	9.381	35.727
30	0.62	38	35	24.293	58.773	1.78	4.122	31.331

Table 9: Prediction sample of experimental data of wax deposition rate of waxy crude oil in Kenli Oilfield (Case I) [34]

Number	X_1	X_2	X_3	X_4	X_5	X_6	X_7	X_8
1	0.9	41	38	24.794	41.324	0.84	4.625	17.033
2	0.9	42	38	22.707	37.845	0.84	6.128	21.261
3	0.18	42	38	4.541	37.845	0.84	3.591	28.390
4	0.62	42	38	15.643	37.845	0.84	5.458	22.837
5	0.62	40	38	18.88	45.677	0.84	2.766	13.575

Table 10: Training sample of experimental data of wax deposition rate of waxy crude oil in Huachi operation area (Case II) [35]

Number	Y_1	Y_2	Y_3	Y_4	Y_5	Y_6	Y_7	Y_8
1	33	30	29.31	5.69	0.29	2.24	2.62	11.90
2	35	32	25.84	1.51	0.09	1.23	2.10	11.63
3	35	32	25.66	2.50	0.15	1.64	2.10	10.91
4	35	32	25.49	4.96	0.29	2.24	2.10	10.13
5	35	32	25.40	7.42	0.44	2.60	2.10	9.75
6	35	32	25.35	9.87	0.58	2.87	2.10	9.50
7	35	32	25.30	14.78	0.88	3.23	2.10	9.19
8	37	34	22.34	4.36	0.29	2.24	1.52	7.51
9	38	35	20.97	4.10	0.29	2.24	1.16	6.54
10	40	37	18.79	1.10	0.09	1.23	0.63	6.40
11	40	37	18.67	1.83	0.15	1.64	0.63	6.00
12	40	37	18.56	3.64	0.29	2.24	0.63	5.57
13	40	37	18.51	5.44	0.44	2.60	0.63	5.36
14	40	37	18.48	7.24	0.59	2.87	0.63	5.22
15	40	37	18.44	10.84	0.88	3.23	0.63	5.05
16	44	41	14.81	2.91	0.30	2.24	0.34	6.20
17	45	42	14.04	2.76	0.30	2.24	0.34	6.77
18	46	43	13.33	2.63	0.30	2.24	0.37	7.20
19	48	45	12.05	2.38	0.30	2.24	0.46	7.11
20	49	46	11.47	2.27	0.30	2.24	0.52	5.95

(Continued)

Table 10 (continued)

Number	Y_1	Y_2	Y_3	Y_4	Y_5	Y_6	Y_7	Y_8
21	35	30	25.72	5.01	0.29	3.72	2.62	15.96
22	37	32	23.03	1.35	0.09	2.08	2.10	14.42
23	37	32	22.77	2.22	0.15	2.75	2.10	13.54
24	37	32	22.53	4.40	0.29	3.72	2.10	12.59
25	37	32	22.35	8.72	0.59	4.76	2.10	11.81
26	37	32	22.28	13.04	0.88	5.35	2.10	11.42
27	42	37	16.98	1.00	0.09	2.08	0.51	9.92
28	42	37	16.82	1.65	0.15	2.75	0.51	9.31
29	42	37	16.58	4.88	0.44	4.33	0.51	8.33
30	42	37	16.54	6.49	0.59	4.76	0.51	8.12
31	42	37	16.5	9.71	0.88	5.35	0.51	7.86
32	42	35	16.78	3.29	0.29	7.44	0.77	11.30
33	40	30	19.09	3.74	0.29	7.44	1.93	22.46

Table 11: Prediction sample of experimental data of wax deposition rate of waxy crude oil in Huachi operation area (Case II) [35]

Number	Y_1	Y_2	Y_3	Y_4	Y_5	Y_6	Y_7	Y_8
1	37	32	22.41	6.56	0.44	4.33	2.10	12.11
2	40	35	18.71	3.66	0.29	3.72	0.88	9.60
3	42	37	16.66	3.27	0.29	3.72	0.51	8.66
4	37	30	22.72	4.43	0.29	4.73	2.62	18.09
5	45	35	14.39	2.83	0.30	7.44	0.64	16.43

Innovation

1. Aiming at correcting the defects of the traditional ENN, such as the tendency to fall into the local minimum value and weak generalization ability, an IRSA is proposed to improve the prediction model of ENN, which can optimize the weights and thresholds initialized by the traditional ENN, so the prediction accuracy of the model can be greatly improved.

2. The RSA cannot achieve a good balance between global search and local search, and it will fall into the local optimal solution. PWLCM is introduced to initialize the population and expand the search space of the population. A novel IRSA is proposed.